Available online at www.sciencedirect.com
SCIENCE DIRECT®
Physica C 412–414 (2004) 795–800
PHYSICA C
www.elsevier.com/locate/physc

High critical current YBCO coated conductors based on IBAD MgO

P.N. Arendt *, S.R. Foltyn, L. Civale, R.F. DePaula, P.C. Dowden, J.R. Groves, T.G. Holesinger, Q.X. Jia, S. Kreiskott, L. Stan, I. Usov, H. Wang, J.Y. Coulter

Superconductivity Technology Center, Los Alamos National Laboratory, P.O. Box 1663, MS K763, Los Alamos, NM 87545, USA

Received 29 October 2003; accepted 2 December 2003
Available online 1 June 2004

Abstract

This report describes recent developments of second-generation $Y_1Ba_2Cu_3O_{7-\delta}$ (YBCO) coated conductors deposited on biaxially textured MgO templates. The materials system architecture implemented to achieve high critical currents in YBCO films is described. The average full-width at half maximum (FWHM) in-plane texture obtained for MgO films processed on meter-length tapes is 7°, while that for the YBCO films is 3°. The best YBCO in-plane values approach 2° and the out-of-plane values approach 1°. Critical currents (1 cm wide tapes, 75 K, self field) have attained 423 A for 7 cm length and 233 A for 50 cm length tapes.

PACS: 74.72.B; 74.80.B; 81.15.–z
Keywords: YBCO coated conductor; Ion-beam assisted deposition; Biaxial texture

1. Introduction

Ion-beam assisted deposition of MgO (IBAD MgO) [1,2] is a promising approach for fabricating long-length template films for high critical current YBCO coated conductors [3]. Its promise lies in the fact that very good biaxial texture can be obtained with films only 10 nm thick [4]. Because it is much thinner than other high quality IBAD templates (e.g. yttria-stabilized zirconia (YSZ) is ~500–700 nm thick) [5,6], IBAD MgO requires additional layers not needed when IBAD YSZ is implemented. Fig. 1 is a cross-section transmission electron micrograph (TEM), which provides a comparison of the non-superconducting layers presently needed to successfully fabricate high quality YBCO films using these two templates. In both cases, a buffer layer is required to ameliorate lattice mismatch and potential deleterious interfacial reactions between the IBAD and the YBCO films. Fig. 1(a) illustrates IBAD YSZ and its accompanying buffer (CeO_2) film. In Fig. 1(b) although the IBAD MgO is much thinner than the IBAD YSZ, several thin, non-superconducting layers are present in addition to the $SrTiO_3$ buffer. These extra layers have differing functions, which either exist in the IBAD YSZ or are not required

* Corresponding author. Tel.: +1-505-665-8358; fax: +1-505-665-3164.
E-mail address: arendt@lanl.gov (P.N. Arendt).

0921-4534/$ - see front matter © 2004 Elsevier B.V. All rights reserved.
doi:10.1016/j.physc.2003.12.074

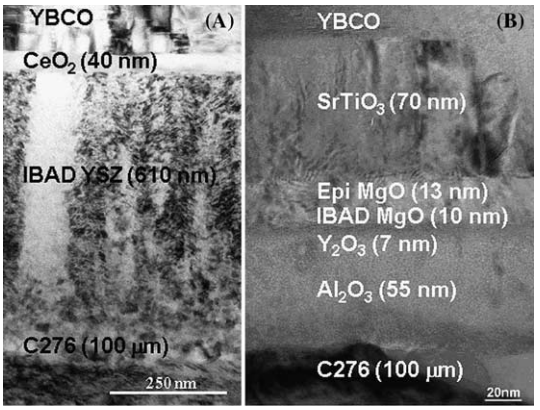

Fig. 1. TEM cross-sections of coated conductor architectures based on (a) IBAD YSZ or (b) IBAD MgO biaxial templates.

for its implementation in coated conductors. Specifically in addition to its template function, the thick IBAD YSZ also acts as a barrier, inhibiting transition metal elements in the Ni-alloy substrate (e.g. Ni, Cr, Mn, Mo, etc.) from diffusing into the superconductor during the high-temperature processing needed to heteroepitaxially deposit the buffer and YBCO layers. The presence of small quantities of such elements will degrade the superconducting properties of YBCO [7]. In this report, we will demonstrate that the thin IBAD MgO and its requisite buffer do not prevent such diffusion from occurring, with a result that the YBCO is not superconducting. Two possible solutions can be employed to ameliorate the diffusion. One is to employ a thick buffer or buffer stack (~250–350 nm), as is normally done with rolling-assisted biaxial textured metal substrates [8]. A second option is to insert a layer below the IBAD MgO, which would inhibit the diffusion. We have chosen to use this latter method where this layer corresponds to the bottom Al_2O_3 layer in Fig. 1(b). One reason for choosing Al_2O_3 is that, for the processing temperatures relevant to YBCO film deposition, it has very low diffusion coefficients for transition metals and oxygen [9]. Also, since it need not be oriented, it may be deposited at ambient temperatures allowing it to be amorphous or nanocrystalline [10]. Films that are nanocrystalline or amorphous have been demonstrated to be superior diffusion barriers than larger grain polycrystalline films of equivalent thickness [11]. Larger grain films are a result of deposition at high temperatures, as are required for buffer layers.

The thin dark layer seen at the top of the lighter Al_2O_3 layer in Fig. 1(b) is Y_2O_3. It functions as a nucleation layer for the IBAD MgO and, in conjunction with the ion-assist beam, promotes (0 0 1) texture normal to the substrate surface as well as biaxial texture for the IBAD MgO film, at its initial nucleation phase. Again, such a layer is not required for IBAD YSZ as both its out-of-plane and in-plane textures slowly evolve with increasing film thickness [12], on a variety of crystalline or amorphous platforms.

The thin homoepitaxial MgO film on top of the IBAD is present because the MgO lattice is damaged by the IBAD processing. The lattice constant at the surface of the IBAD MgO film varies from 0.43 to 0.44 nm. The thin homoepitaxial layer acts as a buffer film restoring the surface lattice constant to that of the bulk lattice parameter (0.421 nm) [13]. This reduces the possibility of strain related misorientations occurring in the subsequent $SrTiO_3$ or $SrRuO_3$ buffer layers whose lattice parameters are 0.391 and 0.393 nm, respectively.

2. Experimental

Hastelloy C276 substrates (0.1 mm thick × 1 cm wide) are electro polished in a reel-to-reel system capable of mean surface roughness values of 0.5 nm RMS [14]. This system includes stations for substrate cleaning before polishing, several electro polishing cells, and several rinse stations to further clean the polished tape. The polished and cleaned tapes are cut and spot welded into ~1.1 m loops and mounted in a dual ion-beam assisted deposition system for continuous mode processing [15]. The length of the deposition zone is 10 cm with two tape loops mounted side by side for simultaneous coating. The sputter targets used for the first three film depositions are 99.99% aluminum, 99.9% yttrium and 99.9% magnesia, respectively. All of the depositions in this system are done at ambient temperature. The system is opened after each deposition run to change the targets. The ion sputter beam energies during these depositions is

~900 eV. Sufficient oxygen partial pressures are provided to ensure that the films are fully oxygenated. Film stoichiometries are confirmed by Rutherford backscattering spectroscopy. During the Al_2O_3 deposition, a 125 eV Ar^+ assist is used to optimize the film density. This film is deposited to a thickness of 50–80 nm at a rate of 0.2 nm/s. Without using an ion assist, the Y_2O_3 deposition is performed next at a rate of 0.08 nm/s, to a film thickness of ~7 nm. The IBAD MgO is deposited at a rate of 0.05 nm/s to a total film thickness of 10–12 nm. The Ar^+ assist beam energy is 750 eV and the ion to molecule deposition ratio is ~0.8–1.0. The impinging angle for the Ar^+ arriving at the deposition zone is ~45°.

The IBAD coated tapes are then transferred to a loop drive RF magnetron sputter deposition system where a 12–15 nm thick homo epitaxial MgO film is deposited at 600 °C. If X-ray texture characterization of a MgO tape is desired (phi scan FWHM of (2 2 0) peak), several cm long pieces are cut from various positions along its length and sputter coated to a final MgO thickness of ~100 nm.

The tapes are then transferred to either of two pulsed-laser deposition (PLD) systems for batch processing of small area (1 cm^2) or continuous process of long-length tapes (up to 1.1 m) [4,16]. Either $SrTiO_3$ or $SrRuO_3$ buffer layers are deposited, followed by 0.5–5.0 μm thick YBCO films. The $SrTiO_3$ is deposited at ~710 °C, the $SrRuO_3$ at ~760 °C and the YBCO at ~760 °C. An oxygen pressure of 200 mTorr is maintained during the PLD depositions. Critical current (I_c) or critical current density (J_c) measurements are performed at 75 K, self field (s.f.) using a 1 μV/cm criterion.

It should be noted that all of these deposition rates are used for research purposes. Substantially higher rates in a tape manufacturing system should produce comparable results.

3. Results and discussion

A multilayer film stack of YBCO/$SrRuO_3$/IBAD MgO/Y_2O_3 was deposited on polished Hastelloy C276. The approximate thickness of each film was 0.5 μm/50 nm/10 nm/7 nm, respectively. An identical stack was made with the addition of an 80 nm thick Al_2O_3 film deposited on the C276 prior to deposition of the remaining layers. Measurements of the YBCO superconducting transition temperatures were made down to 75 K. The YBCO on the first film stack did not exhibit a superconducting transition. The YBCO on the second film stack with the Al_2O_3 addition became fully superconducting at 86 K. SIMS depth profiling of the two sets of films was then performed to elucidate differences in the two sets of films. Fig. 2 illustrates changes in the atomic concentrations of Y and Cr, for the first film stack, as a function of depth. Since standards for each element were not determined prior to the SIMS analysis, the atomic concentrations depicted are approximate and represent an upper limit. Nevertheless, it is seen that the Y signal steadily decreases with increasing depth in the YBCO and then decreases slightly more rapidly when the $SrRuO_3$/IBAD MgO layers are reached. The signal exhibits a slight increase at the Y_2O_3 layer and then continues to taper off slowly into the Hastelloy substrate. As expected, within the substrate, the Cr signal is constant. Because of an artifact of the SIMS measurement, it has a slight increase at the Y_2O_3/Hastelloy interface and then tapers off slowly as the surface of the YBCO is approached. This type of behavior is also exhibited by other substrate elements (e.g. Ni, Mo Mn) [17]. For clarity, these details are not illustrated here.

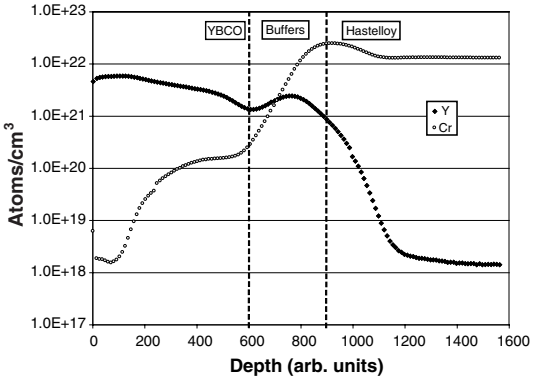

Fig. 2. SIMS depths profile of Y and Cr in YBCO/$SrRuO_3$/IBAD MgO/Y_2O_3 multilayer film stack on Hastelloy C276.

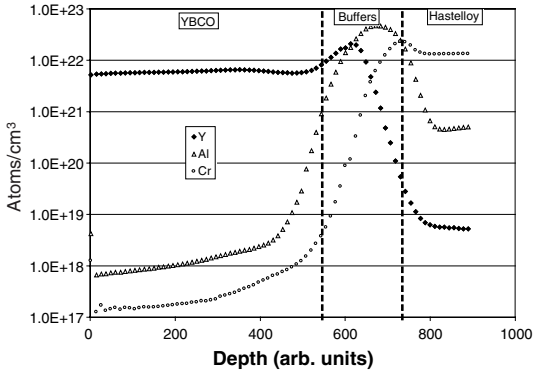

Fig. 3. SIMS depths profile of Y, Cr and Al in YBCO/$SrRuO_3$/IBAD MgO/Y_2O_3/Al_2O_3 multilayer film stack on Hastelloy C276.

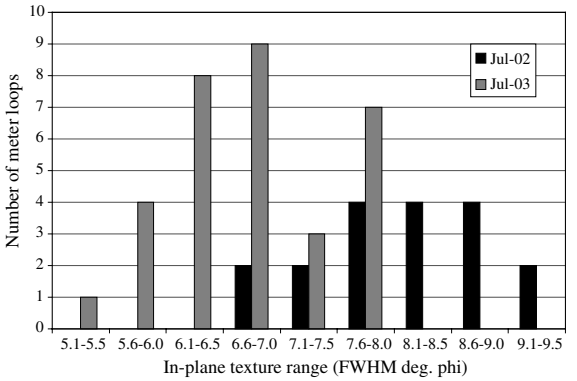

Fig. 4. Histogram of in-plane textures obtained for 1.1 m tapes processed in the 12 months preceding July 2002 and July 2003.

Fig. 3 illustrates changes in the atom densities of Y, Cr, and Al as a function of depth in the second film stack. Here the Y signal remains constant throughout the YBCO film, exhibits a slight decrease at the buffer layer and an increase at the Y_2O_3 layer. It then decreases rapidly in the Al_2O_3 layer and remains at a low, constant value in the substrate. In comparison with Fig. 2, the Cr signal decreases more rapidly going from the substrate into the YBCO film and is over an order of magnitude lower at the YBCO surface. This behavior is also exhibited for the other Hastelloy elements [17]. Thus, the SIMS and superconducting transition temperature data support the hypothesis that the alumina layer performs as a barrier to prevent elements diffusing from the substrate into the YBCO film. In the second film stack, the constant Y signal exhibited throughout the YBCO layer also indicates that the Al_2O_3 plays a role in keeping elements from diffusing out of the YBCO into the substrate. SIMS data, not illustrated here, confirms that the Cu and Ba atomic concentrations are also constant when the barrier layer is present. Detailed studies of alumina diffusion barrier capabilities for Hastelloy transition metals are reported elsewhere [10].

In-plane textures obtained over a recent 24 month period for MgO deposited on meter-length tapes are illustrated in Fig. 4 in histogram format. The FWHM values quoted for the meters are averages of measurements taken (MgO(2 2 0) peak) at two or more positions along the length of each tape. There are two reasons for the improvement of the texture distributions from July 2002 to July 2003. In the earlier reporting period, the starting metal substrate surface finishes averaged ~3 nm RMS, while in the second period the finishes were improved to <1 nm RMS (atomic force microscopy, 5×5 μm scan area). Surface finish differences of this amount have been shown to influence the in-plane texture of IBAD MgO [18]. A second reason is that the divergence of the assist-ion beam was reduced between the first and second reporting periods. Reductions in assist-beam divergence have been shown to effectively reduce the texture of IBAD films [19]. Improvements have been made in the assist-beam divergence beyond those outlined in [19]. The particular methods used to further reduce the assist beam divergence will be the subject of a future report.

The two texture distributions of Fig. 4 were averaged for each year long period and are shown in Fig. 5. Texture distributions obtained during earlier time periods were also averaged and are illustrated in Fig. 5. These data are summarized for the history of our program's development efforts for processing of meter lengths of IBAD MgO. The large texture reductions realized early in the first half of 2001 are attributed to improvements in control of the deposition parameters.

Small sample (~1 cm^2) batch processing of the YBCO and buffer films on IBAD MgO has also been improved recently to the point where

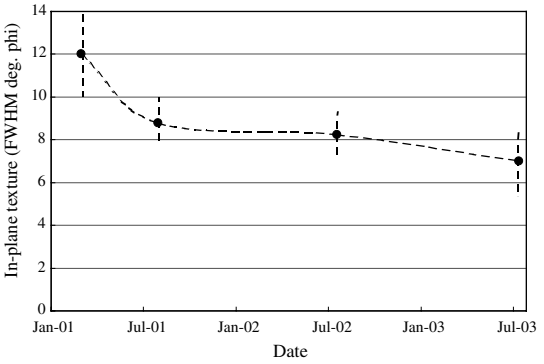

Fig. 5. History of in-plane texture improvement for IBAD MgO 1.1 m tapes. The vertical dashed lines indicate the range of textures measured for all of the meters processed since the previously reported value. The solid circles are the average FWHM values for all of the meters processed during each reporting period.

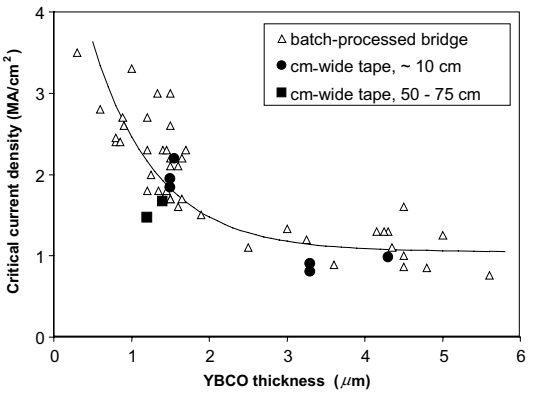

Fig. 6. YBCO J_c vs. thickness for microbridge data and 1 cm wide tapes deposited on the IBAD MgO coated conductor architecture. The solid curve is a fit to data for YBCO films on single crystal YSZ and MgO substrates.

the superconductor has in-plane textures (YBCO(1 0 3) peak) several degrees better than those of the starting template [3]. The average YBCO in-plane texture values of $2.7 \pm 0.5°$ FWHM quoted for the films described in [3] were obtained using tapes with MgO in-plane textures which averaged 6.8° FWHM. The best YBCO values of 1.2° FWHM normal to the film plane were also obtained from these same tapes. J_c vs. thickness values for these YBCO films are also quite remarkable in that they compare quantitatively to values obtained for YBCO films deposited on single-crystal YSZ or MgO substrates [3]. Previously, a superconductor multilayer architecture was reported as necessary to improve the overall supercurrent capability of thick YBCO films (>1.5 μm) for coated conductors [20]. However, the data reported in [3] is for single layer YBCO films up to 3.5 μm thick with no observed degradation in the J_c with the increased thickness. This is attributed to the fact that the recent IBAD MgO architecture results in an overall smoother template on which the YBCO and buffer films are deposited. Recently, single layer YBCO films up to 5 μm thick have been reported to exhibit the same J_c correlation with single-crystal substrates [21]. This microbridge data is illustrated in Fig. 6 with the open triangles. The solid curve is a fit to data for YBCO films on single-crystal YSZ and MgO substrates.

The batch processing improvements used to obtain the above microbridge results were then used to deposit YBCO/buffers on longer length, 1 cm wide tapes. Depositions on 20 cm length pieces (~10 cm measured) resulted in I_c values of 265, 276, 292, 298, and 319 A. On two meter-length sections, the measured I_cs were 173 A (70 cm) and 175 A (72 cm). A 52 cm length within the latter tape had an I_c of 233 A. All of these tapes utilized a YBCO thickness range of ~1.5–3 μm. To demonstrate higher current, a 4.3 μm YBCO film was deposited on a 20 cm length and an I_c of 423 A ($J_c = 1$ MA/cm^2) was measured. The J_c data for these tapes is included in Fig. 6 and is seen to compare favorably with the microbridge results.

Acknowledgements

This work was funded by the US Department of Energy, Office of Energy Efficiency and Renewable Energy Program, Distributed Energy and Electricity Reliability Program.

References

[1] C.P. Wang, K.B. Do, M.R. Beasley, T.H. Geballe, R.H. Hammond, J. Appl. Phys. 71 (1997) 2955.
[2] J.R. Groves, P.N. Arendt, S.R. Foltyn, R.F. DePaula, E.J. Peterson, T.G. Holesinger, J.Y. Coulter, R.W. Springer,

C.P. Wang, R.H. Hammond, IEEE Trans. Appl. Supercond. 9 (1999) 1964.
[3] S.R. Foltyn, P.N. Arendt, Q.X. Jia, H. Wang, J.L. MacManus-Driscoll, S. Kreiskott, R.F. DePaula, L. Stan, J.R. Groves, P.C. Dowden, Appl. Phys. Lett. 82 (2003) 4519.
[4] J.R. Groves, P.N. Arendt, S.R. Foltyn, Q.X. Jia, T.G. Holesinger, H. Kung, E.J. Peterson, R.F. Depaula, P.C. Dowden, L. Stan, L.A. Emmert, J. Mater. Res. 16 (2001) 2175.
[5] Y. Iijima, K. Kakimoto, M. Kimura, K. Takeda, T. Saitoh, IEEE Trans. Appl. Supercond. 11 (2001) 2816.
[6] P.N. Arendt, S.R. Foltyn, J.R. Groves, R.F. DePaula, P.C. Dowden, J.M. Roper, J.Y. Coulter, Appl. Supercond. 429 (1996) 4.
[7] M.F. Yan, W.W. Rhodes, P.K. Gallagher, J. Appl. Phys. 63 (1988) 821.
[8] X. Li, M.W. Rupich, W. Zhang, N. Nguyen, T. Kodenkandath, U. Schoop, D.T. Verebelyi, C. Thieme, M. Jowett, P.N. Arendt, S.R. Foltyn, T.G. Holesinger, T. Aytug, D.K. Christen, M.P. Paranthaman, Physica C 390 (2003) 249.
[9] W.D. Kingery, H.K. Bowen, D.R. Uhlmann, Introduction to Ceramics, 2nd Ed., John Wiley and Sons, New York, 1976.
[10] I. Usov, P. Arendt, L. Stan, R. DePaula, S. Foltyn, H. Wang, S. Foltyn, P. Dowden, J. Mater. Res. 19 (2004) 1175.
[11] A. Gupta, H. Wang, A. Kvit, G. Duscher, J. Narayan, J. Appl. Phys. 93 (2003) 5210.
[12] J. Dzick, J. Wiesmann, J. Hoffmann, K. Heinemann, F. Garcia Moreno, A. Isaev, H.C. Freyhardt, W. Lechner, IEEE Trans. Appl. Supercond. 9 (1999) 2248.
[13] P.N. Arendt, DOE Superconductivity Program for Electrical Systems, Annual Peer Review, Washington, DC, August 1–3, 2001.
[14] S. Kreiskott, P.N. Arendt, L.E. Bronisz, S.R. Foltyn, V. Matias, Supercond. Sci. Tech. 16 (2003) 613.
[15] P.N. Arendt, S.R. Foltyn, J.R. Groves, R.F. DePaula, P.C. Dowden, J.M. Roper, J.Y. Coulter, Appl. Supercond. 4 (1996) 429.
[16] S.R. Foltyn, P.N. Arendt, P.C. Dowden, R.F. DePaula, J.R. Groves, J.Y. Coulter, Q.X. Jia, M.P. Maley, D.E. Peterson, IEEE Trans. Appl. Supercond. 9 (1999) 1519.
[17] P.N. Arendt, DOE Superconductivity Program for Electrical Systems, Annual Peer Review, Washington, DC, July 23–25, 2003.
[18] J.R. Groves, P.N. Arendt, S.R. Foltyn, Q.X. Jia, T.G. Holesinger, L.A. Emmert, R.F. DePaula, P.C. Dowden, L. Stan, IEEE Trans. Appl. Supercond. 13 (2003) 2651.
[19] P.N. Arendt, J.R. Groves, S.R. Foltyn, Q.X. Jia, E.J. Peterson, R.F. DePaula, P.C. Dowden, M. Ma, Mater. Res. Soc. Symp. Proc. 585 (2000) 67.
[20] Q.X. Jia, S.R. Foltyn, P.N. Arendt, J.F. Smith, Appl. Phys. Lett. 82 (2003) 4519.
[21] S.R. Foltyn, DOE Superconductivity Program for Electrical Systems, Annual Peer Review, Washington, DC, July 23–25, 2003.